Colloids and Surfaces B: Biointerfaces 160 (2017) 92–100

Contents lists available at ScienceDirect

Colloids and Surfaces B: Biointerfaces

journal homepage: www.elsevier.com/locate/colsurfb

Protocols

Effects of temperature and PEG grafting density on the translocation of PEGylated nanoparticles across asymmetric lipid membrane

Zuoheng Zhang[a,b,1], Xubo Lin[a,c,1], Ning Gu[a,b,*]

[a] State Key Laboratory of Bioelectronics, Jiangsu Key Laboratory for Bio materials and Devices, School of Biological Science and Medical Engineering, Southeast University, Nanjing 210096, PR China
[b] Collaborative Innovation Center of Suzhou Nano-Science and Technology, Suzhou Key Laboratory of Biomaterials and Technologies, Suzhou 215123, PR China
[c] Department of Integrative Biology & Pharmacology, Medical School, The University of Texas Health Science Center at Houston, TX 77030, USA

ARTICLE INFO

Article history:
Received 15 June 2017
Received in revised form 20 August 2017
Accepted 5 September 2017
Available online 6 September 2017

Keywords:
Temperature
PEG grafting density
Translocation of nanoparticles across membrane
Flip-flop
Coarse-grained molecular dynamics simulation

ABSTRACT

Plasma membrane internalization of nanoparticles (NPs) is important for their biomedical applications such as drug-delivery carriers. On one hand, in order to improve their half-life in circulation, PEGylation has been widely used. However, it may hinder the NPs' membrane internalization ability. On the other hand, higher temperature could enhance the membrane permeability and may affect the NPs' ability to enter into or exit from cells. To make full use of their advantages, we systematically investigated the effects of temperature and PEG density on the translocation of PEGylated nanoparticles across the plasma asymmetric membrane of eukaryotic cells, using near-atom level coarse-grained molecular dynamics simulations. Our results showed that higher temperature could accelerate the translocation of NPs across membranes by making lipids more disorder and faster diffusion. On the contrary, steric hindrance effects of PEG would inhibit NPs' translocation process and promote lipids flip-flops. The PEG chains could rearrange themselves to minimize the contacts between PEG and lipid tails during the translocation, which was similar to 'snorkeling effect'. Moreover, lipid flip-flops were affected by PEGylated density as well as NPs' translocation direction. Higher PEG grafting density could promote lipid flip-flops, but inhibit lipid extraction from bilayers. The consequence of lipid flip-flop and extraction was that the membranes got more symmetric.

1. Introduction

Understanding the interactions between nanoparticles (NPs) and cell membranes is important for improving NPs' biomedical applications in diagnosis/treatment and avoiding NPs' potential nanotoxicity. Biological effects of NPs caused by size [1], hydrophobictiy [2], shape [3,4], surface charge density [5,6], surface modification [7–9] and multi-particle cooperation [10] have been widely explored by simulations and experiments. Some simulation about these factors were summarized systematically in the review of Ding et al. and they pointed out it was better to consider all the aspects when designing functional nanomaterials [11]. NPs' translocation ability across the biomembranes is one of critical parameters for their biomedical applications [10,12]. Higher NP translocation efficiency and lower membrane disruption are two important factors for this purpose. Results showed that the transition from partly to fully wrapped states of a single NP was determined by the balance between the contact energy of adhesion and curvature energy of membrane [13,14].

It is well-known that the transmembrane distribution of lipids is inherently asymmetric in most animal cells [15]. Some previous studies have researched the translocation of NPs across the asymmetric membranes [1,16,17]. Phosphatidylcholine (PC) is the most abundant class of lipids in the outer leaflet, and the inner leaflet mostly consists of phosphatidylethanolamine (PE) in the plasma membrane of eukaryotic cells [18]. Several studies [19–21] have been conducted in atomic-scale computational studies, which confirmed that the asymmetric distribution of membrane can cause a nonzero potential drop from outer leaflet to inner leaflet.

Temperature provides one way to modulate NP translocation efficiency. On the one hand, properties of NPs' surface molecules could be regulated by temperature [22]. Previous papers reported

* Corresponding author at: State Key Laboratory of Bioelectronics, Jiangsu Key Laboratory for Bio materials and Devices, School of Biological Science and Medical Engineering, Southeast University, Nanjing 210096, PR China.
E-mail address: guning@seu.edu.cn (N. Gu).
[1] These authors contributed equally to this work.

http://dx.doi.org/10.1016/j.colsurfb.2017.09.013
0927-7765/

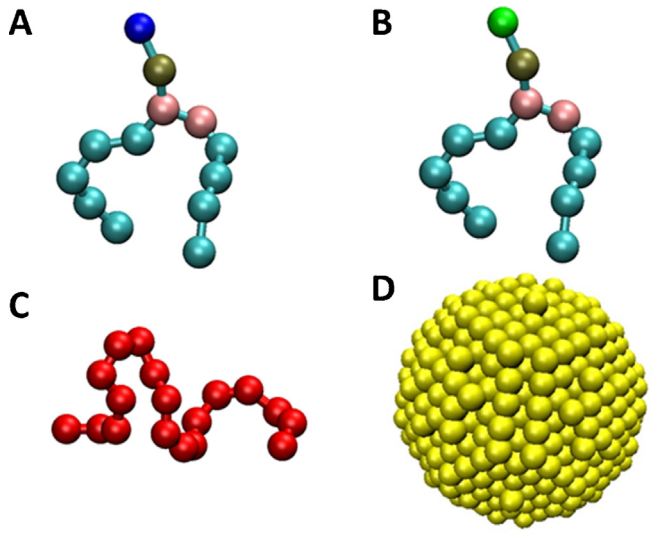

Fig. 1. Martini-based snapshots of POPC (A) and POPE (B) molecules. Two molecules were composed of amine groups (blue), choline groups (green), phosphate groups (brown), glycerol groups (pink) and carbon chains (cyan). (C) Snapshot of a coarse-grained PEG chains including $\boldsymbol{N}$ = 18 monomers and corresponding to a molecular weight of 838 Da. (D) Snapshot of a coarse-grained naked NP core whose diameter was $\boldsymbol{d}\approx$6 nm. (For interpretation of the references to colour in this figure legend, the reader is referred to the web version of this article.)

some temperature-sensitive drug-delivery carrier could control the cellular uptakes [23]. On the other hand, temperature could also tune the membrane properties. For instance, Lin et al. [24] indicated that the NPs' heating can increase the nearby supported lipids' and water's thermal motions. Some experiments also indicated that higher temperature could promote cell uptake of NPs [25–27].

Magnetic NPs could be heated via an external alternating magnetic field. Recent achievements of magnetic hyperthermia in cancer therapy of clinical trials are very promising [28]. The reasonable range of temperature might be below 70 °C in clinical applications and animal experiments according previous researches [28–30]. Besides, magnetic NPs have also been widely utilized as drug carriers to improve localized enrichment [31]. In order to reduce the toxicity and overcome the short circulation half-life of NPs, polyethylene glycol (PEG) have been extensively used [32]. Previous experiments [33] and simulations [34,35] claimed that a steric barrier for NPs provided by PEG molecules can suppress the wrapping of NPs by biomembranes. In the present paper, we investigated the effects of temperature above 37 °C and PEG density on the translocation of NPs across membrane by dynamics simulations to provide insights for the hyperthermia and drug delivery.

2. Model and methods

2.1. MARTINI force field

A coarse grained (CG) force field, MARTINI, was employed for all simulations in this paper for the larger length-scale and longer time-scale system. MARTINI CG force field retained both computational efficiency and sufficient structural details [36]. More details of models can be found in the paper of Marrink et al. [37,38]

2.2. Model of PEGylated NP

Here, we chose a C1-type bead, which was the same as the tails of lipids, to construct a hydrophobic NP. 1566 Beads were stacked in a face-centered cubic (FCC) manner to form a nearly spherical NP and the diameter of the NP was $\boldsymbol{d}\approx$6 nm (Fig. 1D). All beads of NP within 1 nm were added with a constraint to maintain a rigid NP [39]. The next stage was to modify the naked NPs with the PEG chains (Fig. S1). Each PEG monomer (O-C-C) consisting of three heavy atoms was represented as a single bead and all the force field parameters of PEG followed the researches of Lee et al. [40,41] The length of a polymeric PEG chain was denoted by $\boldsymbol{N}$ that was the amount of monomer groups. A single PEG chain in our configuration included $\boldsymbol{N}\approx$18 monomers, corresponding to a molecular weight of 838 Da [35] (Fig. 1C). Surface beads grafted by PEG polymers were randomly selected according to the given the grafting density ($\sigma_{\boldsymbol{p}}$). We chose $\boldsymbol{\sigma_p}\approx$0.4, 0.8, 1.2 chains nm^{-2} corresponding to 45, 90 and 135 chains on each NP [34]. Finally, simulations of three PEGylated NPs for equilibration were performed at 310 K for 100 ns.

2.3. Model of POPC and POPE

In our system, the membrane formed by adjoined POPC and POPE monolayers were asymmetric, which can mimic the outer and inner leaflets of plasma membranes [19–21]. POPE lipid contained a primary amine (Q_d bead) instead of a choline moiety (Q_0 bead) in POPC (Fig. 1A, B). We constructed a membrane with 242 lipids in POPC monolayer and 256 lipids in POPE monolayer according to the analysis in the Section 2 of supplementary information (**SI**). It seemed that their mass density and electrostatic potential were affected by temperatures (**Fig. S3**). In consideration of the size of the PEGylated NPs, we enlarged the smaller system to four-fold one (966 POPC molecules and 1024 POPE molecules) which were large enough for the translocation across membranes.

2.4. System configuration

To facilitate the following description, the mid-plane of the lipid bilayer was defined as the x-y plane and the perpendicular direction to the plane was represented by z-axis [2]. Along the z-axis, the lipid leaflet with the larger z values was the upper lipid leaflet composed of POPC lipids and another one was the lower lipid leaflet composed of POPE lipids. Our researches mainly focused on the auxiliary drug delivery during magnetic hyperthermia in cancer therapy. There were different opinions on the temperature of hyperthermia although some clinical trials suggested that 46 °C was sufficient [28]. Other researchers assumed the temperature was at least 55 °C for clinical applications [29] and heated up to more than 70 °C in animal experiments [30]. Therefore, we chose 310 K, 320 K and 330 K which were under reasonable temperature range in our researches.

Subsequently, the PEGylated NP was added into an equilibrated POPC/POPE asymmetric bilayer system and was initially placed ~10 nm above the center-of-mass of the membrane. We considered this distance would not have significant impact on both PEGylated NP and membranes because they have no direct contact with each other. After energy minimization, a pre-equilibration run of 150 ns in each system was processed to remove steric conflicts at 310 K, 320 K and 330 K. During the whole equilibrations, a harmonic potential was applied between the COM of NP and membrane with a force constant of 1500 kJ mol^{-1} nm^{-2} to guarantee the immobile distance between the NP and the membrane. Finally, a constant force ($\boldsymbol{f}$=700 kJ mol^{-1} nm^{-1}) was used to pull the PEGylated NP across the membrane after pre-equilibration simulations to speed up the process.

All simulations were performed with GROMACS 4.5.4 simulation package [42]. A cutoff of 1.2 nm was used for van der Waals interactions. Both Lennard-Jones potential and Coulombic potential were smoothly shifted to zero between 0.9 nm and 1.2 nm to reduce the cutoff noise. The default value of relative dielectric constant was 15. Considering the small simulation system, we believe that the heating of NPs can affect the whole system. Therefore,

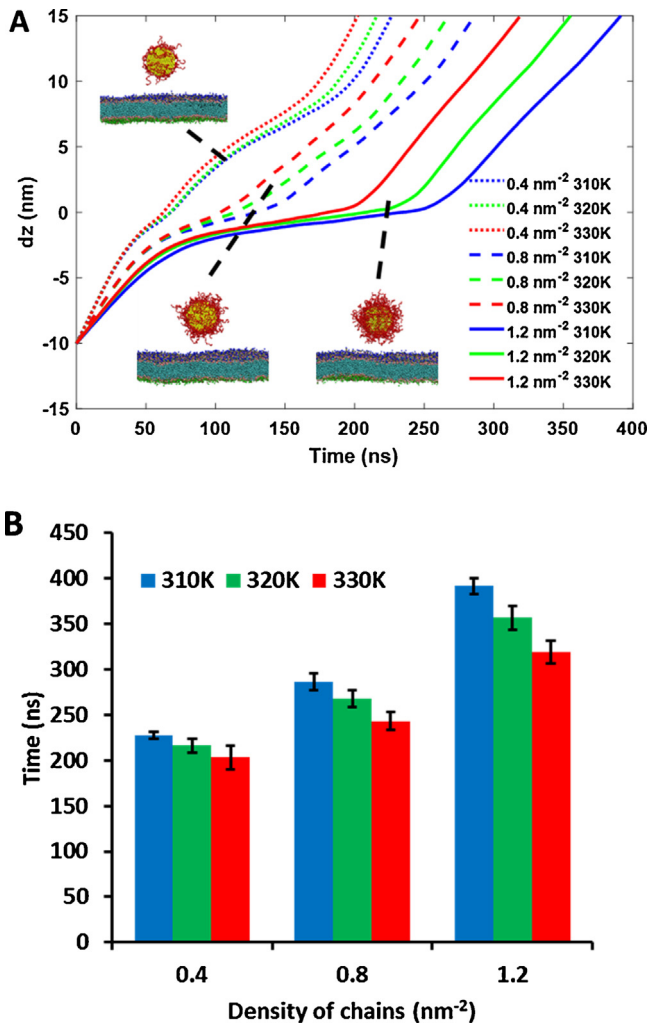

Fig. 2. Effects of the temperature and grafting density on the translocation across membrane of NPs. (A) The y-axis (dz) represented the distance between the COMs of asymmetric membrane and PEGylated NP. Blue, green and red corresponded to 310 K, 320 K and 330 K respectively. Dot, dash and solid styles of the curves denoted 0.4 nm^{-2}, 0.8 nm^{-2} and 1.2 nm^{-2} grafting density respectively. (B) The elapsed time when the distance between the COMs of asymmetric membrane and PEGylated NP with different grafting densities reached 15 nm. At this distance, all of the NPs can cross the asymmetric membrane completely. All above each result for different temperatures and different grafting densities was calculated from three independent simulations. (For interpretation of the references to colour in this figure legend, the reader is referred to the web version of this article.)

Lipids, water and the PEGylated NPs were coupled separately to Berendsen heat baths at $\boldsymbol{T}$=310 K, 320 K and 330 K, with a coupling constant $\boldsymbol{\tau}$ =1 ps. Berendsen coupling schemes for both pressure (semi-isotropic, coupling constant of 0.2 ps, compressibility in the x-y plane of 3×10^{-5} bar^{-1} and in the z-axis of zero) were used to establish a NPT ensemble for imitation of biological condition. 450 ns separated MD simulations for different temperatures and different grafting density were carried out three times independently with a time step of 10 fs.

3. Results and discussion

3.1. The effects of temperature and grafting density on the translocation rate of PEGylated NPs

3.1.1. The rate of translocation of NPs

The plots in Fig. 2A reflected the variation of distance between COM of NP and membrane with different time under external force ($\boldsymbol{f}$=700 kJ mol^{-1} nm^{-1}). The NPs were placed ~10 nm above lipid membranes as the initial configuration, which was corresponding to ~−10 nm of vertical coordinate. In addition, we also tried the external force of $\boldsymbol{f}$=600 kJ mol^{-1} nm^{-1}. The results under two different force were similar, but the translocation process was very slow for higher grafting density and lower temperature (Fig. S4). Therefore, the following analysis was based on the results under external force of $\boldsymbol{f}$=700 kJ mol^{-1} nm^{-1}.

Grafting PEG chains on the surface of NPs regulated the properties from hydrophilicity to hydrophobicity. The interaction between membrane and polymers was affected by hydrophobicity significantly in previous work [43]. At lower PEG density (0.4 nm^{-2}), enhanced exposure of naked core to the surface would make the entire NP more hydrophobic. Therefore, when NPs approached to lipid membranes, the velocity decreased gradually corresponding to the declined gradient segment of plot in Fig. 2A. Subsequently, as the NPs moved into lipid membranes, the attractive force between exposed NP core and tails of lipid molecules facilitated that NPs enter into the hydrophobic region of lipid membranes [2]. Similarly, this interaction also inhibited further translocation of NPs from hydrophobic region to lower leaflet. Finally, when NPs separated from lower leaflet to water phase, the movement speed increased gradually. This was also similar to the single-walled carbon nanotubes research of Pogodin et al. [44] At higher PEGylated density (1.2 nm^{-2}), the NP core was almost covered by hydrophilic PEG chains. The whole process of translocation only consisted of two successive segments of obvious deceleration and acceleration because the effects of hydrophobicity of NP core on translocation decreased with increasing PEG density.

According to the snapshots of systems (Fig. S5), when the distance between COM of NP and membrane reached 15 nm, all of the NPs were separated from the membranes. Fig. 2B showed the time of NPs from the initial position to where the NPs were separated from the membranes. It was proved that heating promoted the translocation of NPs across membranes, but the increasing grafting density inhibited this process on the contrary. We also chose the NP with 0.4 nm^{-2} grafting density as an example to depict the PMF change during the translocation process at 310 K and 330 K as shown in Fig. S6 according to the previous works [7,45]. The lowest energy points of the two profiles were ~0 nm, which meant the NPs tended to maintain at the middle of the membranes instead of translocating across the membranes. The change of the PMF was lighter at 330 K than the change at 310 K. The difference demonstrated higher temperature could decrease the free energy barrier of the translocation process. This was consistent with previous results of experiments [22,25–27] and simulations [34]. More intense lateral diffusion and weaker order property were two main factors to facilitate translocation of NPs across membranes at higher temperature, and the steric barrier of PEG chains was the reason for inhabitation.

3.1.2. Lateral diffusion

To characterize the dynamic properties of phospholipid bilayers, we focused on the lateral diffusion coefficient $\boldsymbol{D_L}$ [46].

$$\boldsymbol{D_L} = \lim_{t \to \infty} \frac{1}{2dt} \left\langle |\boldsymbol{r}(t) - \boldsymbol{r}(0)|^2 \right\rangle \quad (1)$$

$\boldsymbol{d}$=2 and $\boldsymbol{r}(t)$ and $\boldsymbol{r}(0)$ should be projected onto the membrane plane to yield the lateral mean square displacement (LMSD). Then, the diffusion coefficient was fitting by linear regression of the LMSD.

Fig. 3 showed the averaged LMSD plots for the COM of POPC and POPE lipids at different temperature. All curves tended to satisfy the Einstein Eq. (1). POPE lipids were restrained by the intra- and intermolecular hydrogen bonds caused by primary amine, which therefore reduced the motion of the lipids in the bilayer plane. Fur-

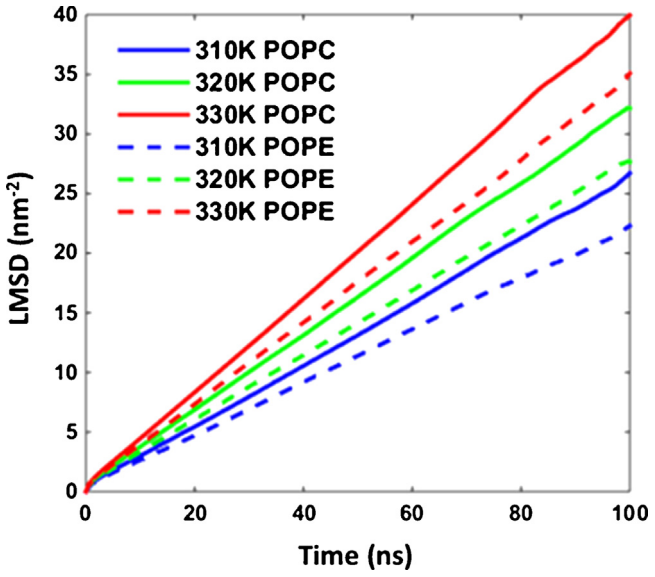

Fig. 3. Average LMSD plots for the COM of POPC and POPE lipids at different temperature. Blue, green and blue represented 310 K, 320 K and 330 K respectively. Solid and dash styles of plots were used to distinguish POPC and POPE lipids. (For interpretation of the references to colour in this figure legend, the reader is referred to the web version of this article.)

thermore, the rising temperature resulted in faster change of LMSD. The difference in LMSD caused by various types of bilayer lipids was a little weaker than that caused by rising temperature.

With linear fitting the LMSD plots, we calculated the lateral diffusion coefficients $\boldsymbol{D_L} = (6.564 \pm 0.004) \times 10^{-7}$ $cm^2\,s^{-1}$, $(7.931 \pm 0.002) \times 10^{-7}$ $cm^2\,s^{-1}$ and $(9.949 \pm 0.001) \times 10^{-7}$ $cm^2\,s^{-1}$ for POPC lipids at 310 K, 320 K and 330 K respectively. Meanwhile, the lateral diffusion coefficients for POPE lipids were $\boldsymbol{D_L} = (5.490 \pm 0.005) \times 10^{-7}$ $cm^2\,s^{-1}$, $(6.779 \pm 0.001) \times 10^{-7}$ $cm^2\,s^{-1}$ and $(8.519 \pm 0.001) \times 10^{-7}$ $cm^2\,s^{-1}$. Generally, the lateral diffusion coefficients of our simulations were under the rational range $(1 \times 10^{-7} - 10 \times 10^{-7}$ $cm^2\,s^{-1})$ [47,48] and the increasing trend with temperatures was consistent with previous results [49]. In our simulations, lateral diffusion coefficients for POPE lipids were less than POPC lipids at the same temperature, which denoted that POPE lipids possessed lower fluidity than POPC lipids.

3.1.3. Order parameter

The second-rank order parameter [37] for Martini coarse-grained force field can be derived from:

$$\boldsymbol{P}_2 = \left\langle \frac{1}{2}(3\boldsymbol{cos}^2\boldsymbol{\theta} - 1) \right\rangle \quad (2)$$

where $\boldsymbol{\theta}$ was the angle between the direction of the bond and the bilayer normal. Perfect alignment with the bilayer normal was denoted by $\boldsymbol{P}_2$ =1, perfect anti-alignment with $\boldsymbol{P}_2$ = −0.5 and $\boldsymbol{P}_2$ between −0.5 and 1 indicated the random orientation. $\leq\cdots\geq$ meant the order parameter of each bond was calculated by averaging over 50–150 ns. The order parameters of bonds were displayed in Fig. 4. The tendencies of our order parameters were very similar to Marrink's previous simulations [37]. The phosphate-choline/primary amine bond and the glycerol linkage were predominantly parallel to the surface of membrane corresponding to negative order parameters. For the tails of lipids, the order parameters decreased from ~0.45 at the glycerol-carbon bond to ~0.1 at the end of tails, which was consistent with previous experimental results [50].

The order parameter of phosphate-choline bond in POPC was much larger than phosphate-primary amine bond in POPE, which meant the phosphate-primary amine bond in POPE had a more parallel orientation to the membrane. This phenomenon was caused by the stronger hydrogen bonds between phosphate and primary amine. The difference of order parameters between POPC and POPE lipids increased for tails. The probable cause was the denser conformation generates more steric effects. Furthermore, molecular thermodynamic movement was another important factor affecting the order properties. As shown in Fig. 4, the absolute values of order parameters decreased slowly when the temperature of systems rose from 310 K to 330 K. This illustrated that lipid molecular distributed in more random orientation.

3.1.4. Morphology of PEGylated NPs

The conformation of grafting chains can transit from 'mushroom' regime with lower grafting density to 'brush' regime with higher grafting density, which was observed in many researches [51,52]. The continuous change of conformation was also appeared in our simulations for PEG polymers, although there was not a sharp boundary between these two regimes. We calculated the particle number density distribution profiles and normalization of PEG chains in radial direction (the details of algorithm and analysis were shown in section 7 of SI). Fig. S8 and Fig. S9 showed higher temperature and higher grafting density led to less PEG atoms concentrated near the surface of the naked NPs core and more PEG atoms extended to water phase. The effect of grafting density was more significant compared with temperatures. Besides, the peak value of each number density profile was at the fixed position regardless of temperature or grafting density, which was consistent with previous results [53].

The radius $\boldsymbol{R}$, which was defined as the mean distance between the farthest atom of each PEG chain and the center of the naked NP core, increased with grafting density and temperature (Table 1). The average volume occupied by a single chain $\boldsymbol{V_{polymer}}$ was calculated according to the work of Li et al. [34] and we obtained similar results. $\boldsymbol{V_{polymer}}$ decreased with the increment of $\boldsymbol{\sigma_p}$, which indicated more degrees of freedom and less steric barrier. This would affect the structure of PEG in membranes (more details in later sections).

The results on grafted chains' radii of gyration $\boldsymbol{R_g}$ and end-to-end distance $\boldsymbol{R_{ee}}$ (**Fig. S1**) further confirmed our above observations. Higher grafting density or temperature induced larger $\boldsymbol{R_g}$ and $\boldsymbol{R_{ee}}$, due to stronger steric interaction and molecular thermodynamic movement respectively. However, the increasing tendency of $\boldsymbol{R_{ee}}$ had some abnormalities. This might be resulted from that $\boldsymbol{R_{ee}}$ just be considered as the absolute length between two end beads in a single PEG chain and ignored the direction of the chains (Fig. S10A). Therefore, we proposed a more effective radial projection of end-to-end distance $\boldsymbol{R_{ee-project}}$ in Fig. S10B. Increasing $\boldsymbol{R_{ee-project}}$ denoted the PEG chains extended to water phase in radial direction at higher temperature or more grafted density (Table 1).

3.2. The effects of grafting density on lipid distribution

3.2.1. The structural changes of PEG chains

Gkeka et al. and Van Lehn et al. have reported that the surface of NP coated with ligands which consists of hydrophobic chains and a negatively charged hydrophilic end groups would rearrange to form optimal contacts with the lipid bilayer, leading to the so-called snorkelling effect [54,55]. In our simulations, we also observed similar snorkelling effect during the translocation of NP across membranes with lower grafting density (Fig. 5Ad), though the PEG chains were electroneutral. The mechanism was that stretching PEG chains toward two sides of membranes could maximize hydrophobic contact of NP core with alkane tails of lipids and hydrophilic contact of PEG chains with water and polar head group.

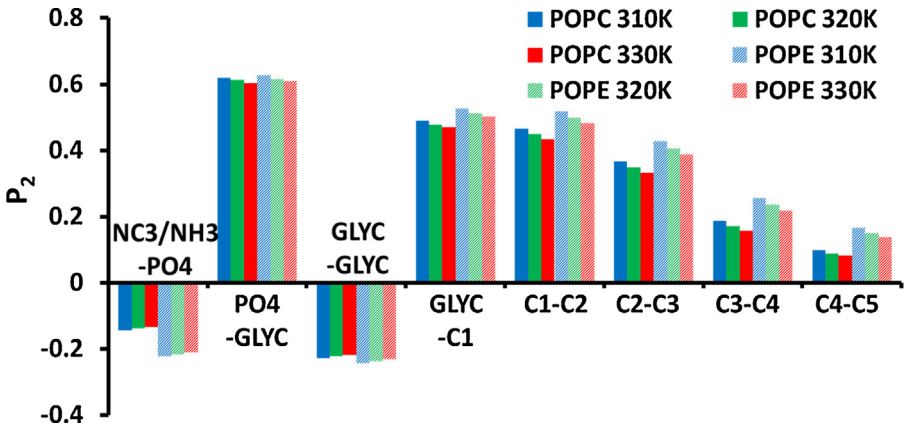

Fig. 4. P_2 order parameters of consecutive bonds for POPC and POPE lipids at different temperatures. Blue, green and blue represented 310 K, 320 K and 330 K respectively. The shadows on the histograms of POPE lipids were used to distinguish two different lipids. (For interpretation of the references to colour in this figure legend, the reader is referred to the web version of this article.)

Table 1
Effects of grafting density σ_p (or number of chains M) and temperature T on the structures of PEGylated NPs [a].

σ_p	T	M	R [b]	$V_{polymer}$ [c]	R_g [d]	R_{ee} [e]	$R_{ee-project}$ [f]
(nm^{-2})	(K)		(nm)	(nm^3)	(nm)	(nm)	(nm)
0.4	310 K	45	4.044 ± 0.088	3.652 ± 0.401	2.842 ± 0.019	2.083 ± 0.085	0.298 ± 0.119
	320 K	45	4.092 ± 0.082	3.873 ± 0.383	2.857 ± 0.021	2.095 ± 0.107	0.359 ± 0.097
	330 K	45	4.118 ± 0.091	3.997 ± 0.433	2.870 ± 0.018	2.073 ± 0.116	0.413 ± 0.108
0.8	310 K	90	4.457 ± 0.060	2.867 ± 0.167	3.213 ± 0.017	2.169 ± 0.067	0.812 ± 0.066
	320 K	90	4.502 ± 0.064	2.992 ± 0.183	3.232 ± 0.021	2.222 ± 0.076	0.847 ± 0.067
	330 K	90	4.524 ± 0.069	3.055 ± 0.199	3.245 ± 0.020	2.222 ± 0.076	0.878 ± 0.077
1.2	310 K	135	4.750 ± 0.055	2.488 ± 0.115	3.489 ± 0.019	2.308 ± 0.052	1.148 ± 0.070
	320 K	135	4.762 ± 0.051	2.515 ± 0.108	3.499 ± 0.016	2.316 ± 0.056	1.161 ± 0.057
	330 K	135	4.789 ± 0.048	2.572 ± 0.103	3.522 ± 0.015	2.339 ± 0.051	1.192 ± 0.060

[a] All above results were calculated by averaging 101 coordinate files uniformly extracted from trajectory files for 50–150 ns.
[b] The radius of PEGylated NPs.
[c] The average volume occupied by a single PEG chain.
[d] Chains' radii of gyration.
[e] End-to-end distance of a single PEG chain.
[f] The radial projection of end-to-end distance.

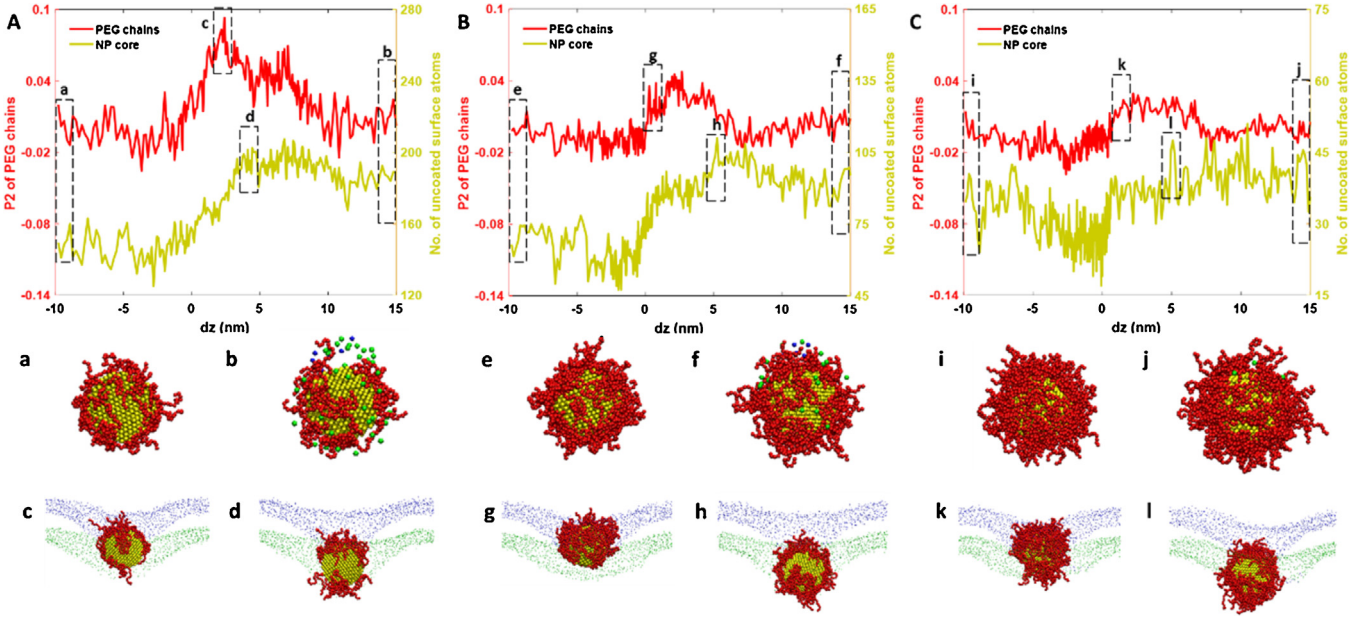

Fig. 5. Plots of P_2 of PEG chains and number of uncoated NPs core surface atoms by PEG chains, and some snapshots of NPs, choline groups, amine groups of membranes. Plots (A), (B), (C) corresponded to 0.4 nm^{-2}, 0.8 nm^{-2} and 1.2 nm^{-2} grafting density respectively. The x-axis was the distance between COMs of NP and membrane. The snapshots were chosen at the beginning (a, e, i), at the end (b, f, j) and at the time when structure of PEG chains (c, g, k) and number of uncoated NPs core surface atoms changed (d, h, l). Green and blue beads represented choline groups and amine groups respectively, other parts of lipids were not shown for clarity. (For interpretation of the references to colour in this figure legend, the reader is referred to the web version of this article.)

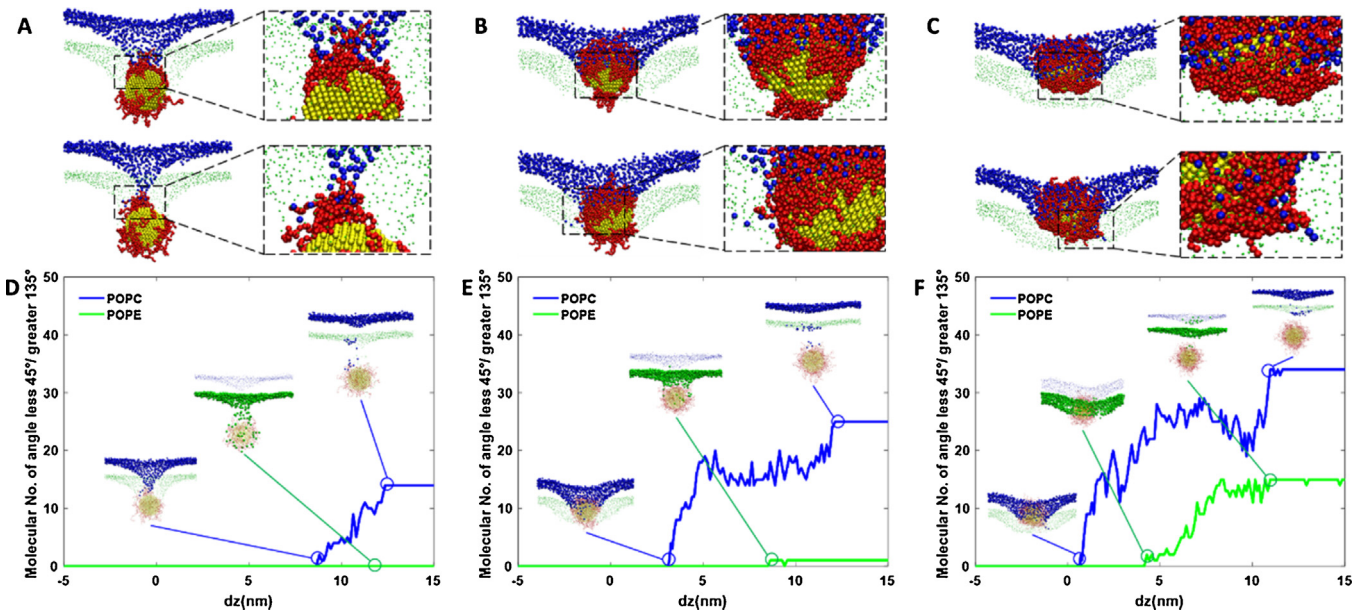

Fig. 6. Snapshots of NPs, choline groups, amine groups of membranes and plots of molecular number of angle less 45° for POPE lipids or greater 135° for POPC lipids with the z dimension of bilayers. Snapshots of (A), (B), (C) corresponded to 0.4 nm^{-2}, 0.8 nm^{-2} and 1.2 nm^{-2} grafting density. The top of snapshots showed the structure before lipids flip-flop occurred. The bottom of snapshots showed the structure when POPC moved to opposite layer. Plots of (D), (E), (F) denoted the number of lipids flip-flops for NPs with 0.4 nm^{-2}, 0.8 nm^{-2} and 1.2 nm^{-2} grafting density. The x-axis was the distance between COMs of NP and membrane. Green and blue beads represented choline groups and amine groups respectively, other parts of lipids were not shown for clarity. (For interpretation of the references to colour in this figure legend, the reader is referred to the web version of this article.)

The PEG chains were more perpendicular to x-y plane in membranes instead of random orientation in water phase because of snorkelling effect. Second-rank order parameter ($\boldsymbol{P}_2$) was also used to illustrate this process. The red plots represented $\boldsymbol{P}_2$ of PEG chains with 0.4 nm^{-2}, 0.8 nm^{-2} and 1.2 nm^{-2} grafting density during the translocation at 310 K in Fig. 5A, B and C respectively. Before NPs contacted with membranes, all $\boldsymbol{P}_2$ of PEG chains were generally stable at ~0 corresponding to random orientation in water phase (Fig. 5a, e, i). After NPs touched with membranes, $\boldsymbol{P}_2$ plots obviously rose with 0.4 nm^{-2}, 0.8 nm^{-2} grafting density because of the snorkelling effect. PEG chains became more alignment with the bilayer normal (Fig. 5c d, g, h). However, the orientation of NPs with 1.2 nm^{-2} grafting density had slighter variation. The main factor was steric barrier caused by dense distribution of PEG chains inhibited the structural changes. After translocation of NPs across membranes, $\boldsymbol{P}_2$ fell back to previous values (Fig. 5b, f, j).

Furthermore, we also analysed the number of uncoated atoms by PEG chains on the NPs' surface. The number of uncoated surface atoms of NPs maintained at a lower level, when PEG chains randomly distributed in water. It was obvious that the lower grafting density (~140 at 0.4 nm^{-2} in Fig. 5A) would result in much more uncoated surface atoms than these at higher density (~35 at 1.2 nm^{-2} in Fig. 5C). As NPs crossed into membranes, the yellow plots rose gradually because alignment of PEG chains with the bilayer normal and more lipid molecules adhering to the surface of NPs. Similarly, a few changes of PEG structure induced the slight increase of uncoated surface atoms with 1.2 nm^{-2} grafting density. However, differently from $\boldsymbol{P}_2$ plot, the number of uncoated surface atoms of NPs by PEG chains did not fall back to previous level significantly, after NPs were detached from membrane. We speculated that some atoms of NPs surface were coated by lipids extracted from membranes instead of PEG chains (Fig. 5b, f, j). Furthermore, the changes of PEG structures and surface atoms exposed to hydrophobic core of membrane were related to flip-flops of lipids. This phenomenon would be analysed in the next section.

3.2.2. *The asymmetric transmembrane lipid distribution*

The translocation of lipid molecules from one leaflet to another, which was called flip-flop, was tightly associated with maintaining an asymmetric transmembrane lipid distribution [56]. Exposure of some intracellular lipids to the outside of the cell was related to blood coagulation and apoptosis [57] and the cells can be captured by phagocytes as a presentation of self-antigens to the immune system [58]. Besides, lipid flip-flops can occur with the help of proteins and ATP [59,60] or transmembrane ion density gradient [56].

We observed the translocation of NPs across membranes can cause lipid flip-flops but the lipid exchange occurred in a specific location instead of the whole translocation process. The hydrophilic PEG chains played an important role to determine when the lipids crossed toward another side in our simulations. When PEG chains of NPs with 0.4 nm^{-2}, 0.8 nm^{-2} grafting density were separated into two parts distributed on the two sides of membrane because of snorkelling effect, there was no lipid exchange between POPC and POPE leaflets though membrane had obvious deformation (top of Fig. 6A, B). It was resulted from that uncoated NP core atoms blocked the translocation of lipids to another side. Lipid flip-flops would not occur until PEG chains connected upper leaflets and lower leaflets (bottom of Fig. 6A, B, C). Flip-flops mediated by hydrophilic atoms in our work were consistent with previous results [56,61].

Afterwards we defined a computational method to quantify the lipids flip-flops in the whole translocation process approximately (details of calculation were shown in section 9 of SI), though it was difficult to obtain very accurate results unless the naked eye [62]. The blue and green plots of Fig. 6D, E, F approximately represented the number of POPC and POPE flip-flops when the PEGylated NPs translocated from POPC side to POPE side. It was obvious that the flip-flops occurred later for NPs with lower grafting density. If only the distance between COMs of NPs and membranes was just over ~0 nm, some POPC lipids would translocate to lower leaflet for 1.2 nm^{-2} grafting density. However, the flip-flop of POPC for 0.4 nm^{-2} took place at the COMs distance of ~8 nm where the NP was about to be detached from membrane. Similar phenomenon

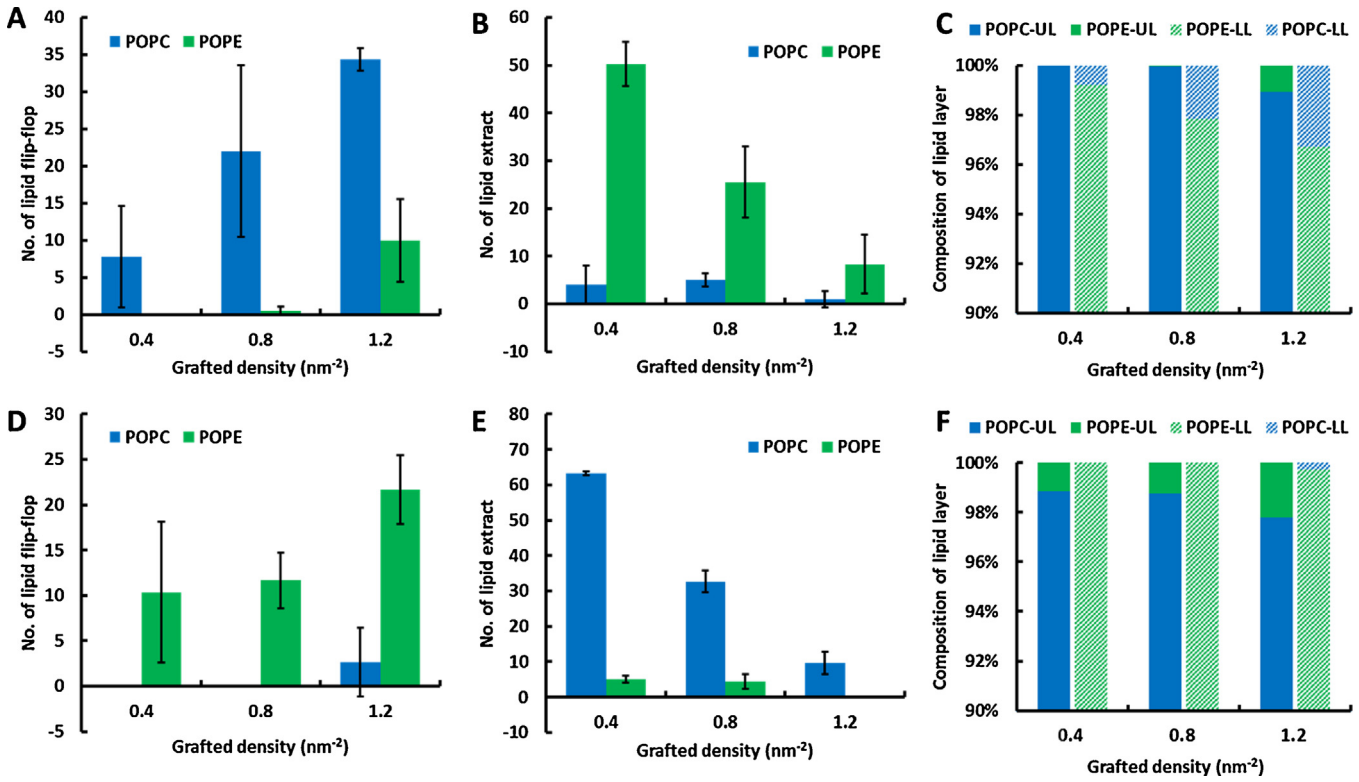

Fig. 7. Lipid flip-flop (A) and extraction (B) with different grafting density under the translocation of NPs from POPC side to POPE side. (D) and (E) denoted the lipid flip-flop and extraction in the opposite direction. Blue and green bars represented that POPC lipids and POPE lipids moved to another leaflet or were pulled out from the membrane respectively. The proportion of POPC and POPE lipids in two leaflets of membrane after the translocation of NPs from upper leaflet to lower leaflet (C) and the opposite direction (F). Blue and green bars represented the proportion of POPC and POPE lipids in upper leaflet (UL). The shadows on the bars were used to distinguish the values in lower leaflet (LL). All of the results were calculated by averaging three times independent simulations at 310 K. (For interpretation of the references to colour in this figure legend, the reader is referred to the web version of this article.)

was also observed when we reversed direction of the movement of NPs (Fig. S12). The main reason was that more uncoated NP atoms exposed to the hydrophobic core of membrane strongly blocked the lipid flip-flops for lower grafting density. On the contrary, denser PEG chains facilitated the connection between two leaflets, which would make flip-flop easier. Besides, the lipids exchanges between two sides were not fully simultaneously. Lipid flip-flops of POPE happened later than POPC, which was consistent with the results of Oroskar et al. [62]. It might be caused by that NPs bent the bilayers in the direction of movement and pulled the POPC lipids to the opposite side. Besides, we also found if the direction of translocation changed, the results were also reverse (Fig. S12).

We investigated the incidences of flip-flops and extraction of lipids when PEGylated NPs were separated from membranes completely at 310 K (Fig. 7). We found the number of lipid flip-flops increased with grafting density. This tendency might be caused by larger size and more hydrophilic surface of NPs. The similar phenomenon with symmetric lipid membrane were also observed in previous researches [62]. Furthermore, we observed the frequency of POPC flip-flop from upper leaflet to lower leaflet was much higher than that of POPE flip-flop (Fig. 7A). It seemed to be connected with the direction of the movement of NPs. Then we changed the direction and the results were reversed (Fig. 7D).

The hydrophobic properties of NPs can extract lipids from membranes [63,64]. Similarly, the numbers of extracted POPC and POPE lipids were affected by the direction of translocation of NPs. When PEGylated NPs moved from POPC side to POPE side, the most lipids covered on the surface of NPs were POPE (Fig. 7B), but conversely were POPC (Fig. 7E). The results were completely in agreement with the simulation of carbon nanotube [64]. Obviously, with higher grafting density, less lipids were extracted from the membrane, which was caused by smaller hydrophobic area of uncoated NP core.

The consequence of lipid flip-flop and extraction caused by PEGylated NP was that the membranes got more symmetric (Fig. 7C and F). After the translocation of NP from upper leaflet to lower leaflet, the proportion of POPC in lower leaflet (POPC-LL) and POPE in upper leaflet (POPE-UL) would increase and the increase of POPC-LL was much more than that of POPE-UL (Fig. 7C), due to the direction of translocation of NP. The opposite direction would also lead to opposite results (Fig. 7F). Besides, we found higher grafting density would result in more symmetric membranes. It seemed to be minor changes for one translocation. However, the accumulated effects would be very large after many times translocation. The results at 320 K and 330 K were similar to above-mentioned facts (Fig. S13 and Fig. S14). As we know, higher temperature could enhance molecules' thermal motions and thus promote the lipid flip-flop processes. However, as reported in the experiments [65], the flip-flop of lipids such as POPC or POPE happened in the much longer timescale than that of MD simulations. Hence, it was worth mentioning that the lipid flip-flop events reported here were mainly occurred during the NPs' translocation processes, which was mainly regulated by the Van der Waals interactions between PEG and lipids rather than by temperature.

4. Conclusions

Hyperthermia with magnetic NPs showed great promises in tumor treatment, and PEG grafting techniques had been extensively used in drug delivery. Therefore, we investigated the effects of three different temperatures and PEG densities on translocation of PEGylated NPs across the asymmetric membranes using Mar-

tini coarse-grained molecular dynamics simulations. PEG chains tended to spread along the surface of the NP core at lower temperature instead of to stretch to water phase at higher temperature. Besides, more intense lateral diffusion and weaker order property facilitated translocation of NPs across membranes. The drug therapy and magnetic hyperthermia could be combined to facilitate the translocation of nanocarrier into residual tumor cells to kill them. Furthermore, the local temperature around NPs was higher than other area. If we controlled the concentration of NPs to keep the overall temperature in the safe range, it might be used in the drug delivery of normal cells. On the other hand, higher steric barrier with increasing grafting density would inhibit the translocation of NPs, weaken the 'snorkeling effect' of PEG chains and decrease uncoated atoms of NP core. Hence, with higher grafting density, more lipid flip-flops occurred, while less lipids were extracted from the bilayer during PEGylated NPs translocation. It was too hard to solve both problems at once by selecting an appropriate grafting density. Therefore, it was better to achieve a balance between flip-flop and extraction according to the specific application for designing a better PEGylated NP.

Acknowledgements

This work was supported by the National Key Research and Development Program of China (2017YFA0104301), National Basic Research Program of China (2013CB733804, 2011CB933503), the National Natural Science Foundation of China for Key Project of International Cooperation (61420106012), the National High Technology Research and Development Program ("863" Program) of China (2013AA032205) and the Collaborative Innovation Center of Suzhou Nano Science and Technology (SX21400213).

Appendix A. Supplementary data

Supplementary data associated with this article can be found, in the online version, at http://dx.doi.org/10.1016/j.colsurfb.2017.09.013.

References

[1] J. Agudo-Canalejo, R. Lipowsky, Critical particle sizes for the engulfment of nanoparticles by membranes and vesicles with bilayer asymmetry, ACS Nano 9 (2015) 3704–3720.
[2] Y. Li, X. Chen, N. Gu, Computational investigation of interaction between nanoparticles and membranes: hydrophobic/Hydrophilic effect, J. Phys. Chem. B 112 (2008) 16647–16653.
[3] S. Dasgupta, T. Auth, G. Gompper, Shape and orientation matter for the cellular uptake of nonspherical particles, Nano Lett. 14 (2014) 687–693.
[4] Y. Li, M. Kroger, W.K. Liu, Shape effect in cellular uptake of PEGylated nanoparticles: comparison between sphere, rod, cube and disk, Nanoscale 7 (2015) 16631–16646.
[5] Y. Li, N. Gu, Thermodynamics of charged nanoparticle adsorption on charge-Neutral membranes: a simulation study, J. Phys. Chem. B 114 (2010) 2749–2754.
[6] J.Q. Lin, H.W. Zhang, Z. Chen, Y.G. Zheng, Penetration of lipid membranes by gold nanoparticles: insights into cellular uptake, cytotoxicity, and their relationship, ACS Nano 4 (2010) 5421–5429.
[7] Y.F. Li, X.J. Li, Z.H. Li, H.J. Gao, Surface-structure-regulated penetration of nanoparticles across a cell membrane, Nanoscale 4 (2012) 3768–3775.
[8] Z. Shen, M.-P. Nieh, Y. Li, Decorating nanoparticle surface for targeted drug delivery: opportunities and challenges, Polymers 8 (2016) 83.
[9] H.M. Ding, Y.Q. Ma, Role of physicochemical properties of coating ligands in receptor-mediated endocytosis of nanoparticles, Biomaterials 33 (2012) 5798–5802.
[10] M. Raatz, R. Lipowsky, T.R. Weikl, Cooperative wrapping of nanoparticles by membrane tubes, Soft Matter 10 (2014) 3570–3577.
[11] H.M. Ding, Y.Q. Ma, Theoretical and computational investigations of nanoparticle-biomembrane interactions in cellular delivery, Small 11 (2015) 1055–1071.
[12] A. Verma, O. Uzun, Y.H. Hu, Y. Hu, H.S. Han, N. Watson, S.L. Chen, D.J. Irvine, F. Stellacci, Surface-structure-regulated cell-membrane penetration by monolayer-protected nanoparticles, Nat. Mater. 7 (2008) 588–595.
[13] A.H. Bahrami, R. Lipowsky, T.R. Weikl, The role of membrane curvature for the wrapping of nanoparticles, Soft Matter 12 (2016) 581–587.
[14] K.A. Smith, D. Jasnow, A.C. Balazs, Designing synthetic vesicles that engulf nanoscopic particles, J. Chem. Phys. 127 (2007) 084703.
[15] R.B. Gennis, Characterization and Structural Principles of Membrane Proteins, In: Biomembranes: Molecular Structure and Function, Springer New York, New York NY, 1989, pp. 85–137.
[16] H.M. Ding, W.D. Tian, Y.Q. Ma, Designing nanoparticle translocation through membranes by computer simulations, ACS Nano 6 (2012) 1230–1238.
[17] Z.L. Li, H.M. Ding, Y.Q. Ma, Translocation of polyarginines and conjugated nanoparticles across asymmetric membranes, Soft Matter 9 (2013) 1281–1286.
[18] A. Zachowski, Phospholipids In animal eukaryotic membranes – transverse asymmetry and movement, Biochem. J. 294 (1993) 1–14.
[19] A.A. Gurtovenko, I. Vattulainen, Lipid transmembrane asymmetry and intrinsic membrane potential: two sides of the same coin, J. Am. Chem. Soc. 129 (2007) 5358–5359.
[20] A.A. Gurtovenko, I. Vattulainen, Effect of NaCl and KCl on phosphatidylcholine and phosphatidylethanolamine lipid membranes: insight from atomic-scale simulations for understanding salt-induced effects in the plasma membrane, J. Phys. Chem. B 112 (2008) 1953–1962.
[21] A.A. Gurtovenko, I. Vattulainen, Intrinsic potential of cell membranes: opposite effects of lipid transmembrane asymmetry and asymmetric salt ion distribution, J. Phys. Chem. B 113 (2009) 7194–7198.
[22] H. Vihola, A.K. Marttila, J.S. Pakkanen, M. Andersson, A. Laukkanen, A.M. Kaukonen, H. Tenhu, J. Hirvonen, Cell-polymer interactions of fluorescent polystyrene latex particles coated with thermosensitive poly (N-isopropylacrylamide) and poly (N-vinylcaprolactam) or grafted with poly(ethylene oxide)-macromonomer, Int. J. Pharm. 343 (2007) 238–246.
[23] Y. Hiruta, M. Shimamura, M. Matsuura, Y. Maekawa, T. Funatsu, Y. Suzuki, E. Ayano, T. Okano, H. Kanazawa, Temperature-Responsive fluorescence polymer probes with accurate thermally controlled cellular uptakes, ACS Macro Lett. 3 (2014) 281–285.
[24] X.B. Lin, C.L. Wang, M. Wang, K. Fang, N. Gu, Computer simulation of the effects of nanoparticles' adsorption on the properties of supported lipid bilayer, J. Phys. Chem. C 116 (2012) 17960–17968.
[25] A.L. Zhang, Y.X. Guan, L.X. Xu, Theoretical study on temperature dependence of cellular uptake of QDs nanoparticles, J. Biomech. Eng 133 (2011) 6.
[26] L. Thors, C.J. Fowler, Is there a temperature-dependent uptake of anandamide into cells? Br. J. Pharmacol. 149 (2006) 73–81.
[27] J.S. Kim, T.J. Yoon, K.N. Yu, M.S. Noh, M. Woo, B.G. Kim, K.H. Lee, B.H. Sohn, S.B. Park, J.K. Lee, M.H. Cho, Cellular uptake of magnetic nanoparticle is mediated through energy-dependent endocytosis in A549 cells, J. Vet. Sci. 7 (2006) 321–326.
[28] M. Johannsen, U. Gneveckow, K. Taymoorian, B. Thiesen, N. Waldofner, R. Scholz, K. Jung, A. Jordan, P. Wust, S.A. Loening, Morbidity and quality of life during thermotherapy using magnetic nanoparticles in locally recurrent prostate cancer: results of a prospective phase I trial, Int. J. Hyperthermia 23 (2007) 315–323.
[29] I. Hilger, W. Andra, R. Hergt, R. Hiergeist, W.A. Kaiser, Magnetic thermotherapy of breast tumors: an experimental therapeutic approach, Roentgenstr 177 (2005) 507–515.
[30] I. Hilger, R. Hiergeist, R. Hergt, K. Winnefeld, H. Schubert, W.A. Kaiser, Thermal ablation of tumors using magnetic nanoparticles – An in vivo feasibility study, Invest. Radiol. 37 (2002) 580–586.
[31] Q.A. Pankhurst, N.T.K. Thanh, S.K. Jones, J. Dobson, Progress in applications of magnetic nanoparticles in biomedicine, J. Phys. D: Appl. Phys. 42 (2009).
[32] J.M. Harris, R.B. Chess, Effect of pegylation on pharmaceuticals, Nat. Rev. Drug Discovery 2 (2003) 214–221.
[33] M. Schulz, A. Olubummo, W.H. Binder, Beyond the lipid-bilayer: interaction of polymers and nanoparticles with membranes, Soft Matter 8 (2012) 4849–4864.
[34] Y. Li, M. Kroger, W.K. Liu, Endocytosis of PEGylated nanoparticles accompanied by structural and free energy changes of the grafted polyethylene glycol, Biomaterials 35 (2014) 8467–8478.
[35] Y. Li, Y. Hu, Computational investigation of the influence of chain length on the shielding effect of PEGylated nanoparticles, RSC Adv. 4 (2014) 51022–51031.
[36] G. Rossi, L. Monticelli, S.R. Puisto, I. Vattulainen, T. Ala-Nissila, Coarse-graining polymers with the MARTINI force-field: polystyrene as a benchmark case, Soft Matter 7 (2011) 698–708.
[37] S.J. Marrink, A.H. de Vries, A.E. Mark, Coarse grained model for semiquantitative lipid simulations, J. Phys. Chem. B 108 (2004) 750–760.
[38] S.J. Marrink, H.J. Risselada, S. Yefimov, D.P. Tieleman, A.H. de Vries, The MARTINI force field: coarse grained model for biomolecular simulations, J. Phys. Chem. B 111 (2007) 7812–7824.
[39] X.B. Lin, N. Gu, Surface properties of encapsulating hydrophobic nanoparticles regulate the main phase transition temperature of lipid bilayers: a simulation study, Nano Res. 7 (2014) 1195–1204.
[40] H. Lee, R.W. Pastor, Coarse-grained model for PEGylated lipids: effect of PEGylation on the size and shape of self-assembled structures, J. Phys. Chem. B 115 (2011) 7830–7837.
[41] H. Lee, A.H. de Vries, S.J. Marrink, R.W. Pastor, A coarse-Grained model for polyethylene oxide and polyethylene glycol: conformation and hydrodynamics, J. Phys. Chem. B 113 (2009) 13186–13194.
[42] D. Van Der Spoel, E. Lindahl, B. Hess, G. Groenhof, A.E. Mark, H.J. Berendsen, GROMACS: fast, flexible, and free, J. Comput. Chem. 26 (2005) 1701–1718.

[43] M. Werner, J.-U. Sommer, V.A. Baulin, Homo-polymers with balanced hydrophobicity translocate through lipid bilayers and enhance local solvent permeability, Soft Matter 8 (2012) 11714.
[44] S. Pogodin, N.K.H. Slater, V.A. Baulin, Surface patterning of carbon nanotubes can enhance their penetration through a phospholipid bilayer, ACS Nano 5 (2011) 1141–1146.
[45] L. Zhang, M. Becton, X. Wang, Designing nanoparticle translocation through cell membranes by varying amphiphilic polymer coatings, J. Phys. Chem. B 119 (2015) 3786–3794.
[46] B. Liu, X.Y. Li, B.L. Li, B.Q. Xu, Y.L. Zhao, Carbon nanotube based artificial water channel protein: membrane perturbation and water transportation, Nano Lett. 9 (2009) 1386–1394.
[47] J. Tabony, B. Perly, Quasielastic neutron scattering measurements of fast local translational diffusion of lipid molecules in phospholipid bilayers, Biochim. Biophys. Acta Biomembr. 1063 (1991) 67–72.
[48] S. Konig, W. Pfeiffer, T. Bayerl, D. Richter, E. Sackmann, Molecular-dynamics of lipid bilayers studied by incoherent quasi-Elastic neutron-Scattering, J. Phys. II 2 (1992) 1589–1615.
[49] H. Lee, Effects of temperature, salt concentration, and the protonation state on the dynamics and hydrogen-bond interactions of polyelectrolyte multilayers on lipid membranes, Phys. Chem. Chem. Phys. 18 (2016) 6691–6700.
[50] A. Seelig, J. Seelig, Effect of a single cis double bond on the structure of a phospholipid bilayer, Biochemistry 16 (1977) 45–50.
[51] S.T. Milner, Polymer brushes, Science 251 (1991) 905–914.
[52] C.D. Walkey, J.B. Olsen, H. Guo, A. Emili, W.C. Chan, Nanoparticle size and surface chemistry determine serum protein adsorption and macrophage uptake, J. Am. Chem. Soc. 134 (2012) 2139–2147.
[53] J. Lin, H. Zhang, V. Morovati, R. Dargazany, PEGylation on mixed monolayer gold nanoparticles: effect of grafting density, chain length, and surface curvature, J. Colloid Interf Sci. 504 (2017) 325–333.
[54] P. Gkeka, P. Angelikopoulos, L. Sarkisov, Z. Cournia, Membrane partitioning of anionic, ligand-coated nanoparticles is accompanied by ligand snorkeling, local disordering, and cholesterol depletion, PLoS Comput. Biol 10 (2014) e1003917.
[55] R.C. Van Lehn, P.U. Atukorale, R.P. Carney, Y.S. Yang, F. Stellacci, D.J. Irvine, A. Alexander-Katz, Effect of particle diameter and surface composition on the spontaneous fusion of monolayer-protected gold nanoparticles with lipid bilayers, Nano Lett. 13 (2013) 4060–4067.
[56] A.A. Gurtovenko, I. Vattulainen, Molecular mechanism for lipid flip-flops, J. Phys. Chem. B 111 (2007) 13554–13559.
[57] D.L. Daleke, Regulation of transbilayer plasma membrane phospholipid asymmetry, J. Lipid Res. 44 (2003) 233–242.
[58] K. Balasubramanian, A.J. Schroit, Aminophospholipid asymmetry: a matter of life and death, Annu. Rev. Physiol. 65 (2003) 701–734.
[59] R.J. Raggers, T. Pomorski, J.C.M. Holthuis, N. Kalin, G. van Meer, Lipid traffic: the ABC of transbilayer movement, Traffic 1 (2000) 226–234.
[60] H. Leontiadou, A.E. Mark, S.J. Marrink, Antimicrobial peptides in action, J. Am. Chem. Soc. 128 (2006) 12156–12161.
[61] D.P. Tieleman, S.J. Marrink, Lipids out of equilibrium: energetics of desorption and pore mediated flip-flop, J. Am. Chem. Soc. 128 (2006) 12462–12467.
[62] P.A. Oroskar, C.J. Jameson, S. Murad, Simulated permeation and characterization of PEGylated gold nanoparticles in a lipid bilayer system, Langmuir 32 (2016) 7541–7555.
[63] Y.S. Tu, M. Lv, P. Xiu, T. Huynh, M. Zhang, M. Castelli, Z.R. Liu, Q. Huang, C.H. Fan, H.P. Fang, R.H. Zhou, Destructive extraction of phospholipids from Escherichia coli membranes by graphene nanosheets, Nat. Nanotechnol. 8 (2013) 594–601.
[64] E.J. Wallace, M.S.P. Sansom, Blocking of carbon nanotube based nanoinjectors by lipids: a simulation study, Nano Lett. 8 (2008) 2751–2756.
[65] M. Nakano, M. Fukuda, T. Kudo, N. Matsuzaki, T. Azuma, K. Sekine, H. Endo, T. Handa, Flip-flop of phospholipids in vesicles: kinetic analysis with time-resolved small-angle neutron scattering, J. Phys. Chem. B 113 (2009) 6745–6748.